Keyhole Effect in MIMO Wireless Channels: Measurements and Theory

Peter Almers, *Student Member, IEEE*, Fredrik Tufvesson, *Member, IEEE*, and Andreas F. Molisch, *Fellow, IEEE*

***Abstract*— It has been predicted theoretically that for some environments, the capacity of wireless multiple-input multiple-output systems can become very low even for uncorrelated signals; this effect has been termed "keyhole" or "pinhole". In this paper the first unique *measurements* of this effect are presented. The measurements were performed in a controlled indoor environment that was designed to obtain a keyhole channel. We analyze limitations due to measurement imperfections for measurement-based capacity calculations and keyhole investigations. We further present a bound for the higher eigenmodes as a function of the finite measurement signal-to-noise ratio and multipath component leakage. The bound is compared to the measurement results and shows excellent agreement. Finally, we analyze the envelope distribution and, as expected from theory, it follows a *double*-Rayleigh distribution.**

***Index Terms*— Keyhole, pinhole, MIMO, measurements, eigenvalue, double-Rayleigh, capacity.**

I. Introduction

MULTIPLE-INPUT multiple-output (MIMO) wireless communication systems have multi-element antenna arrays at both the transmitter and the receiver side. It has been shown that they have the potential for large information-theoretic capacities, since the system can provide several independent communication channels between transmitter and receiver [1], [2]. In an ideal multipath channel, the MIMO capacity is approximately N times the capacity of a single-antenna system, where N is the smaller of the number of transmit and receive antenna elements. Correlated signals at the antenna elements lead to a decrease in the capacity - this effect has been investigated both theoretically [3], [4], and experimentally [5]. It has recently been predicted theoretically that for some propagation scenarios, the MIMO channel capacity can be low (i.e., comparable to the single-input single-output (SISO) capacity) even though the signals at the antenna elements are uncorrelated [6], [7], [8], [9], [10]. This effect has been termed "keyhole" or "pinhole."

The keyhole effect is related to scenarios where rich scattering around the transmitter and receiver leads to low correlation of the signals, while other propagation effects, like diffraction or waveguiding, lead to a rank reduction of the transfer function matrix. Several previous measurement campaigns have searched for the keyhole effect due to corridors, tunnels, or diffraction in real environments [11]. While some indications for rank reduction have been found, to our knowledge, no unambiguous measurements of a keyhole have been presented in the literature.

In this paper, we present:

- Results of a measurement campaign that for the first time unambiguously shows the keyhole effect experimentally. This includes the measured eigenvalue distribution.
- Separation of correlation and keyhole effects on outage capacity.
- A confirmation by measurements of the theory for the envelope statistics of a keyhole channel.
- An analysis of the impact of measurement noise on keyhole channels.
- An upper bound for the eigenvalue for measured keyhole channels, as a function of the measurement signal-to-noise ratio (SNR).

In [12] we presented measurement results for a 6×6 keyhole (rank-1) channel. In this paper we present extended measurements (including both rank-1 and rank-3 channels) and an extensive analysis including bounds for the capacity of low rank systems. For reference and completeness we also include some results from the letter [12]. The measurements were performed in a controlled indoor environment, where the propagation from one room to the next could only occur through a waveguide or a hole in the wall. The measurement results show almost ideal keyhole properties; the capacity is low, the rank of the transfer matrix is nearly one though the correlation between the antenna elements is low.

The rest of the paper is organized as follows: after some background information on general MIMO channels (Sec. II) and low-rank MIMO channels (Sec. III), we describe the setup of our experiment, describing both environment and measurement equipment in Sec. IV. As noise can never be perfectly excluded in an experiment, Sec. V gives an analysis of its impact on the measured eigenvalue distributions. Sec. VI then derives upper bounds on the higher-order eigenvalues of the transfer function depending on the SNR. Sec. VII finally provides the measurement results, providing data for both the eigenvalue distribution, the information-theoretic capacity resulting from it, and the amplitude distribution. A summary concludes the paper.

Manuscript received February 1, 2005; revised May 3, 2005; accepted October 3, 2005. The associate editor coordinating the review of this paper and approving it for publication was M. Shafi. Parts of this material has been presented at IEEE GlobeCom 2004, San Francisco, USA.

P. Almers is with the Dept. of Electroscience, Lund University, Box 118, SE-221 00 Lund, Sweden (email: Peter.Almers@es.lth.se).

F. Tufvesson is with the Dept. of Electroscience, Lund University, Box 118, SE-221 00 Lund, Sweden (email: Fredrik.Tufvesson@es.lth.se).

A. F. Molisch is with Mitsubishi Electric Research Labs, Cambridge, MA, USA, and also at the Department of Electroscience, Lund University, Box 118, SE-22100 Lund, Sweden (email: Andreas.Molisch@ieee.org).

Digital Object Identifier 10.1109/TWC.2006.05025.

II. MIMO CHANNELS

In this paper we assume a single-user MIMO system with N_{T} transmit and N_{R} receive antenna elements, and flat fading. We use the conventional MIMO model and the received signal vector, $\mathbf{y}$ of size $N_{\mathrm{R}} \times 1$ is written as

$$\mathbf{y} = \mathbf{H}\mathbf{x} + \mathbf{n}, \tag{1}$$

where $\mathbf{H}$ is the channel transfer matrix between the transmitter and the receiver of size $N_{\mathrm{R}} \times N_{\mathrm{T}}$ normalized as,

$$E\left[\|\mathbf{H}\|_{\mathrm{F}}^2\right] = N_{\mathrm{R}} N_{\mathrm{T}}. \tag{2}$$

Further, $\mathbf{x}$ is the transmitted signal vector, and $\mathbf{n} \in \mathcal{CN}\left(\mathbf{0}, \sigma_n^2 \mathbf{I}_{[N_{\mathrm{R}} \times 1]}\right)$ represents noise, where $\mathbf{I}_{[N_{\mathrm{R}} \times 1]}$ is the identity vector.

For equal power allocation between the transmitter elements (no waterfilling), the instantaneous channel capacity [bit/s/Hz] for the channel model in (1) can be calculated as [2]

$$C = \log_2\left(\det\left(\mathbf{I} + \frac{\gamma_{\mathrm{eval}}}{N_{\mathrm{T}}}\mathbf{W}_{\mathbf{H}}\right)\right), \tag{3}$$

or expressed in singular values

$$C = \sum_{k=1}^{K} \log_2\left(1 + \frac{\gamma_{\mathrm{eval}}}{N_{\mathrm{T}}} \left|s_k\left(\mathbf{H}\right)\right|^2\right), \tag{4}$$

where

$$\mathbf{W}_{\mathbf{H}} = \begin{cases} \mathbf{H}\mathbf{H}^{\dagger} & \text{for } N_{\mathrm{R}} \le N_{\mathrm{T}} \\ \mathbf{H}^{\dagger}\mathbf{H} & \text{for } N_{\mathrm{T}} < N_{\mathrm{R}} \end{cases}, \tag{5}$$

$[\cdot]^{\dagger}$ denotes the complex conjugate transpose, and $s_k\left(\mathbf{H}\right)$, is the k :th singular value of $\mathbf{H}$. Further, γ_{eval} is the evaluation SNR, i.e., the signal-to-noise ratio (SNR) that the capacity is evaluated for, defined as

$$\gamma_{\mathrm{eval}} = \frac{E\left[h\left(k,l\right) h^{\dagger}\left(k,l\right)\right]}{E\left[n\left(k\right) n^{\dagger}\left(k\right)\right]} = \frac{\sigma_h^2}{\sigma_n^2} = \frac{1}{\sigma_n^2}, \tag{6}$$

where $E\left[\cdot\right]$ is the expectation[1], $h\left(k,l\right)$ and $n\left(k\right)$ are the k,l :th entry in $\mathbf{H}$ and k :th entry in $\mathbf{n}$, respectively, σ_h^2 is the power of the complex entries in $\mathbf{H}$, and normalized to one from (2). It is assumed that $\mathbf{x}$ has unit energy.

When measuring a MIMO transfer matrix, the measured quantity will consist of contributions not only from multipath components (MPCs) but also from measurement noise. The measured keyhole transfer matrix can be modelled as

$$\mathbf{H}_{\mathrm{meas}} = \mathbf{H}_{\mathrm{key}} + \mathbf{N}_{\mathrm{meas}}, \tag{7}$$

where $\mathbf{N}_{\mathrm{meas}} \in \mathcal{CN}\left(\mathbf{0}, \sigma_{n_{\mathrm{meas}}}^2 \mathbf{I}\right)$ denotes the measurement noise matrix. The measurement SNR, γ_{meas}, can then be defined as

$$\gamma_{\mathrm{meas}} = \frac{E\left[h_{\mathrm{key}}\left(k,l\right) h_{\mathrm{key}}^{\dagger}\left(k,l\right)\right]}{E\left[n_{\mathrm{meas}}\left(k,l\right) n_{\mathrm{meas}}^{\dagger}\left(k,l\right)\right]} = \frac{\sigma_{h_{\mathrm{key}}}^2}{\sigma_{n_{\mathrm{meas}}}^2}. \tag{8}$$

[1]For a deterministic channel, the expectation is taken over the noise realizations only. For a randomly varying channel (as will be considered in the remainder of the paper), the expectation is taken also over the channel realizations.

III. LOW RANK MIMO CHANNELS

The channel capacity is highly dependent on the distribution of the singular values of the normalized channel transfer matrix $\mathbf{H}$, see Eq. 4. The two extreme cases for the singular value distributions of $\mathbf{H}$, in a capacity sense, are:

- equally strong singular values → maximum MIMO capacity, which is $\min\left(N_{\mathrm{R}}, N_{\mathrm{T}}\right)$ times higher than for the SISO channel.
- only one non-zero singular value → minimum MIMO capacity, with only the receiver array gain affecting the capacity.

A skew singular value distribution occurs when the *correlations* of the signals at the receiver and/or transmitter antenna elements are high. However, a skew singular value distribution can also occur with a low correlation between the antenna elements due to the rank of the propagation channel. With zero correlation and only one non-zero singular value it is termed *keyhole* or *pinhole* channel [6], [7], [8], [9].

A. Correlated channels

It is well known that correlation between the antenna elements at the transmitter and/or the receiver reduces the capacity [3], [4], [13], hence the (complex) spatial correlation is an important parameter in describing MIMO channels. A high correlation between receiver and/or transmitter elements could be a result of mutual coupling between elements and/or due to propagation channel effects such as low angular spread, strong line-of-sight (LOS), or a small number of MPCs. In this section we define the most common correlations measures.

The full correlation, $\mathbf{R}$, between all possible combinations of the entries in the channel matrix, $\mathbf{H}$, is defined as

$$\mathbf{R} = E\left[\mathrm{vec}\left(\mathbf{H}\right) \cdot \mathrm{vec}\left(\mathbf{H}\right)^{\dagger}\right], \tag{9}$$

where the operator $\mathrm{vec}(\cdot)$ stacks the columns in the matrix in a column vector. If the receive correlation is the same for all transmitted MPCs, $\mathbf{R}$ can be decomposed as [14], [15]

$$\mathbf{R} = \mathbf{R}_{\mathrm{T}} \otimes \mathbf{R}_{\mathrm{R}}, \tag{10}$$

where $\otimes$ is the Kronecker product. The marginal correlation matrices are

$$\mathbf{R}_{\mathrm{R}} = \frac{1}{N_{\mathrm{T}}} E\left[\mathbf{H}\mathbf{H}^{\dagger}\right], \tag{11}$$

and

$$\mathbf{R}_{\mathrm{T}} = \frac{1}{N_{\mathrm{R}}} E\left[\mathbf{H}^{\dagger}\mathbf{H}\right]^{T}, \tag{12}$$

where $[\cdot]^T$ is the matrix transpose. $\mathbf{R}_{\mathrm{R}}$ and $\mathbf{R}_{\mathrm{T}}$ describe the correlation between the signals at receiver and transmitter elements, respectively. The Kronecker model's tractability for MIMO channel theoretical investigations has made it more widespread than the full correlation model. According to the Kronecker model, the channel, and thus the capacity, is completely determined by the correlations at transmitter and receiver side. In order to compare the capacity reduction due to receive and transmit correlation to the capacity reduction due to the keyhole effect, we use the Kronecker model and the full correlation model described below.

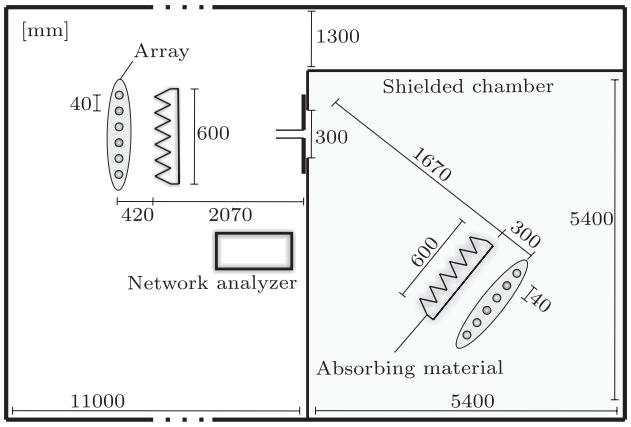

Fig. 1. Overview of the measurement setup.

Correlated MIMO channel snapshots can be generated from both the correlation matrix as

$$\mathrm{vec}\left(\mathbf{H}_{\text{full}}\right) = \mathbf{R}^{1/2} \cdot \mathrm{vec}\left(\mathbf{G}_{\text{full}}\right), \tag{13}$$

and [3]

$$\mathbf{H}_{\text{Kron}} = \frac{1}{\mathrm{tr}\left(\mathbf{R}_{\text{R}}\right)} \mathbf{R}_{\text{R}}^{1/2} \mathbf{G}_{\text{Kron}} \mathbf{R}_{\text{T}}^{T/2}, \tag{14}$$

where the former equation is generally valid, and the latter is valid if the correlation matrix can be decomposed according to (10). $\mathbf{G}_{\text{full}}$ and $\mathbf{G}_{\text{Kron}}$ are $\mathcal{CN}\left(\mathbf{0}, \mathbf{I}\right)$ distributed matrices of size $N_{\text{R}} \times N_{\text{T}}$, and the matrix square root is defined as $\mathbf{A}^{1/2}\left(\mathbf{A}^{1/2}\right)^{\dagger} = \mathbf{A}$.

The full correlation matrix is estimated from the measurements as

$$\hat{\mathbf{R}} = \frac{1}{M} \sum_{m=1}^{M} \mathrm{vec}\left(\mathbf{H}\right) \cdot \mathrm{vec}\left(\mathbf{H}\right)^{\dagger}, \tag{15}$$

and the marginal correlation matrices as

$$\hat{\mathbf{R}}_{\text{R}} = \frac{1}{M N_{\text{T}}} \sum_{m=1}^{M} \mathbf{H}_m \mathbf{H}_m^{\dagger}, \tag{16}$$

and

$$\hat{\mathbf{R}}_{\text{T}} = \frac{1}{M N_{\text{R}}} \sum_{m=1}^{M} \left[\mathbf{H}_m^{\dagger} \mathbf{H}_m\right]^{T}, \tag{17}$$

where M denotes the number of different realizations.

B. Keyhole channels

As mentioned in the introduction, keyhole channels require rich scattering environments around the two arrays without line-of-sight (LOS), together with a low rank connection between the two scattering environments. Examples of keyhole scenarios are

- Local rich scattering environments separated by a large distance [10].
- Rich scattering environments connected by a rank-1 propagation path, see Fig. 1 and [7], [12].
- Rich scattering environments connected via diffractions over an edge.

Since the models in (14) and (13) only considers complex Gaussian channels with spatial correlation, they cannot model a keyhole[2]. In [10] a generalization of the Kronecker model is presented

$$\mathbf{H} = \frac{1}{\sqrt{S}} \mathbf{R}_{\text{R}}^{1/2} \mathbf{G}_{\text{R}} \mathbf{T}^{1/2} \mathbf{G}_{\text{T}} \mathbf{R}_{\text{T}}^{T/2}, \tag{18}$$

where $\mathbf{G}_{\text{R}}$ and $\mathbf{G}_{\text{T}}$ are both i.i.d. complex Gaussian matrices distributed as $\mathcal{CN}\left(\mathbf{0}, \mathbf{I}\right)$, and where $\mathbf{T}^{1/2}$ describes the transfer matrix between the transmitter and receiver environments (i.e., the scatterers around transmitter and receiver), and S is a normalization factor. For a perfect keyhole, e.g., a single-mode waveguide between the transmitter and the receiver environment, $\mathbf{T}^{1/2}$ has rank one. This results in a total channel transfer matrix, $\mathbf{H}$, of rank one as well, even though $\mathbf{R}_{\text{R}}^{1/2}$, $\mathbf{R}_{\text{T}}^{1/2}$, $\mathbf{G}_{\text{R}}$ and $\mathbf{G}_{\text{T}}$ have full rank. The keyhole transfer matrix can then be modeled as [8], [7]

$$\mathbf{H}_{\text{key}} = \mathbf{g}_{\text{R}} \mathbf{g}_{\text{T}}^{\dagger}, \tag{19}$$

where $\mathbf{g}_{\text{R}}, \mathbf{g}_{\text{T}}$ are column vectors distributed as, $\mathbf{g}_{\text{R}}, \mathbf{g}_{\text{T}} \in \mathcal{CN}\left(\mathbf{0}, \sigma_{\text{key}}^2 \mathbf{I}\right)$, and clearly the entries are uncorrelated [7].

When comparing the statistical properties of the entries in the channel matrix of an i.i.d. and a keyhole channel, some interesting differences are found.

- For i.i.d. channels the amplitudes of the entries in the transfer matrix, $\mathbf{H}$, are Rayleigh distributed, but show a double-Rayleigh distribution for the keyhole channels:

$$f_{|h_{\text{key}}|}\left(h\right) = \frac{h}{\sigma_{\text{key}}^4} K_0\left(\frac{h}{\sigma_{\text{key}}^2}\right), \tag{20}$$

- The i.i.d. channel has uncorrelated and independent row and column entries, whereas the keyhole channels has uncorrelated but dependent row and column entries.

IV. Keyhole Measurement Setup

To fulfill the keyhole scenario discussed in the previous section, the measurements were performed with one antenna array located inside a shielded chamber, and the other array in the adjacent room. A hole in the chamber wall was the only propagation path between the two rooms. Fig. 1 shows the layout of the measurement setup. The measurements were performed using a vector network analyzer (Rohde & Schwarz ZVC at $3.5 - 4.0$ GHz and a HP 8720C at $4.9 - 5.4$ GHz). Linear virtual arrays with $6 - 10$ antenna positions and omni-directional conical antennas were used both at the transmitter and the receiver; the measurements were done during night time to ensure a static environment.

Two different rectangular waveguides were attached to the hole as in Fig. 2. The cut-off frequencies of a rectangular waveguide are [17]

$$f_{\text{co}} = \frac{1}{2\sqrt{\mu\epsilon}} \sqrt{\left(\frac{m}{a}\right)^2 + \left(\frac{n}{b}\right)^2}, \tag{21}$$

where a is the width of the wave guide, b is the hight of the waveguide and m, n designate the mode. Further, μ and

[2]In the case of a keyhole, the instantaneous correlation [16] will be able to predict a keyhole. However, the correlation used for the Kronecker model is the *mean* correlation and is not able to predict the keyhole channel. It will therefore overestimate the capacity for MIMO keyhole channels.

Fig. 2. Photo of the waveguide attached to the shielded chamber.

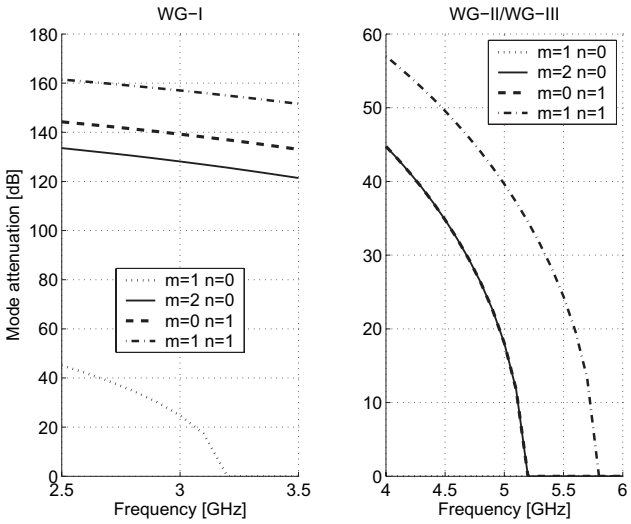

Fig. 3. Propagating mode attenuation.

ϵ are the absolute permeability and the absolute permittivity of the material filling the waveguide (air). The attenuation of a propagating mode is theoretically zero at frequencies above that mode's cut-off frequency, f_{co}. Below the cut-off frequency there is no true propagation but only significant attenuation. It is dependent on the length of the wave guide, z, and the frequency distance to the cut-off frequency of that mode. The attenuation is in the order of $\sim e^{-\delta(f)z}$ where [17]

$$\delta(f) = h\sqrt{1-\left(\frac{f}{f_{\text{co}}}\right)^2}, \tag{22}$$

and

$$h = \sqrt{\left(\frac{m\pi}{a}\right)^2 + \left(\frac{n\pi}{b}\right)^2}. \tag{23}$$

In Fig. 3 the attenuation of the first four propagating modes of the two different wave guides are plotted, where TE10 is $f_{\text{co}} = 3.19$ GHz and $f_{\text{co}} = 2.59$ GHz for WG-I and WG-II/WG-III, respectively. Note that the cut-off frequency, f_{co}, are the same for $(m = 2, n = 0)$ and $(m = 0, n = 1)$ for WG-II/WG-III.

Two additional hole configurations without waveguides were also measured. This gives us the following five setups:

1) A hole of size 47×22 mm with a 250 mm long waveguide attached. We measured 101 complex transfer functions at $3.5 - 4$ GHz, separated by 5 MHz spacing (referred to as WG-I).
2) A hole of size 58×29 mm with a 150 mm long waveguide attached. We measured 51 complex transfer functions at $3.5 - 4$ GHz, separated by 10 MHz spacing (referred to as WG-II).
3) A hole of size 58×29 mm with a 150 mm long waveguide attached. We measured 51 complex transfer functions at $4.9 - 5.4$ GHz, separated with 10 MHz (referred to as WG-III).
4) A hole of size 47×22 mm without waveguide, 101 complex transfer functions separated with 5 MHz at $3.5 - 4$ GHz were taken ("small hole" or SH).
5) A hole of size 300×300 mm without waveguide, 101 complex transfer functions separated with 5 MHz at $3.5 - 4$ GHz were taken ("large hole" or LH).

This means that as the measurement frequency increases in the WG-III measurements, the waveguide shows a transition from a one-moded wave guide to a three-moded waveguide according to Fig. 3.

The received signal was amplified by 30 dB with an external low noise power amplifier to achieve a high measurement SNR. The measurement SNR was estimated to be 26 dB and 21 dB for WG-I and WG-II, respectively, where noise includes thermal noise, interference and possible channel changes during the measurements. The large hole is intended as test measurement, in which we do not anticipate a keyhole effect but rather a full rank channel.

V. Effect of Measurement Noise on Channel Capacity

In this section we analyze the influence of the nonideality of measured transfer functions when calculating the capacity [18], and analyze its effect on our experiment. For keyhole measurements, the measured transfer matrix normally consists of the nominal keyhole transfer matrix, MPC leakage, and noise, so that it can be modelled as in (7) with $\mathbf{N}_{\text{meas}}$ also includes the leakage components as

$$\mathbf{N}_{\text{meas}} = \mathbf{H}_{\text{leak}} + \tilde{\mathbf{N}}, \tag{24}$$

where $\tilde{\mathbf{N}} \in \mathcal{CN}\left(\mathbf{0}, \sigma_{\tilde{n}}^2\, \mathbf{I}\right)$ denotes thermal noise. The MPC leakage describes MPCs propagating between the transmitter and the receiver via other paths than through the keyhole. The leakage matrix together with non-static channel effect (variations of the channel during the measurement time) is modelled by a complex Gaussian matrix $\mathbf{H}_{\text{leak}} \in \mathcal{CN}\left(\mathbf{0}, \sigma_{h_{\text{leak}}}^2 \mathbf{I}\right)$. Using a worst-case scenario (with respect to the resulting deviation from the capacity of an ideal keyhole channel), it is assumed to have independent entries.

Under these assumptions the noise leads to the same destruction of the keyhole effect as leakage. In order to check the effect on the evaluated capacity, we lump the two terms into a single matrix as in (24). Assuming that $\mathbf{H}_{\text{key}}$, $\mathbf{H}_{\text{leak}}$ and $\tilde{\mathbf{N}}$ in (7) and (24) are independent, the measurement SNR (including leakage) from a keyhole measurement point of view, γ_{meas}, can

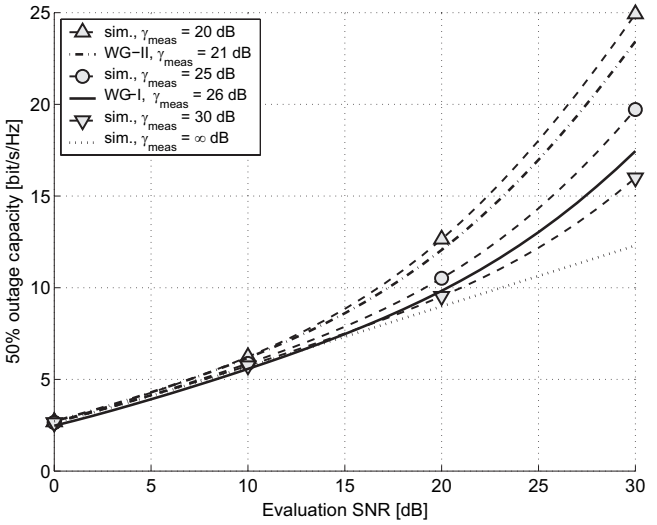

Fig. 4. The estimated capacities for different simulated measurement SNRs $\{20, 25, 30, \infty\}$ versus evaluation SNR [dB] togehter with the measured keyhole with a estimated measurement SNR of $\hat{\gamma}_{\text{meas}} = 21$ dB and $\hat{\gamma}_{\text{meas}} = 26$ dB.

therefore be defined as

$$\gamma_{\text{meas}} = \frac{E\left[h_{\text{key}}(k,l)\, h_{\text{key}}^{\dagger}(k,l)\right]}{E\left[h_{\text{leak}}(k,l)\, h_{\text{leak}}^{\dagger}(k,l)\right] + E\left[\tilde{n}(k,l)\, \tilde{n}^{\dagger}(k,l)\right]}. \tag{25}$$

In Fig. 4 simulations of the 50% outage capacity for three different measurement SNRs versus the evaluated SNR are plotted. Additionally we plot the capacity for our keyhole measurement, which, as mentioned before, has an estimated measurement SNR of $\hat{\gamma}_{\text{meas}} = 26$ dB and $\hat{\gamma}_{\text{meas}} = 21$ dB. From the figure it can be concluded that the SNR of the keyhole *measurement* has to be around 10 dB better than the SNR used in the *evaluation* to give capacity values close to the ideal case. For an evaluation SNR of 15 dB the contribution from noise *and* leakage components has to be 25 dB lower than the components from the keyhole. This is one of the reasons why it can be difficult to find "real-life" keyhole situations, e.g., waveguiding or diffraction, which might explain the difficulty in finding keyholes in previous measurement campaigns. The shielded chamber in our measurements made sure that the leakage was very small, and an evaluation SNR of 15 dB is appropriate in this case.

VI. Upper Bound of Eigenvalues

The rank of an ideal keyhole is one, however a measured keyhole channel has full rank (nonzero eigenvalues) due to thermal noise (and other effects discussed in the previous section). In order to characterize a measured keyhole it is therefore of interest to study the distribution of the singular values (or eigenvalues), especially, the ratio between the largest and second largest singular value, a ratio dependent on the measurement SNR of the keyhole, γ_{meas}.

From the general bound of a sum of two matrices [19]

$$s_{k+l-1}\left(\mathbf{H}_{\text{key}}+\tilde{\mathbf{N}}\right) \leq s_k\left(\mathbf{H}_{\text{key}}\right) + s_l\left(\tilde{\mathbf{N}}\right), \tag{26}$$

the difference between the $k-$th ordered singular value of the measured transfer matrix (7), denoted $s_k\left(\mathbf{H}_{\text{key}}+\tilde{\mathbf{N}}\right)$, and the $k-$th ordered singular value of the keyhole transfer matrix, $s_k\left(\mathbf{H}_{\text{key}}\right)$, is limited by [19], [20]

$$\left|s_k\left(\mathbf{H}_{\text{key}}+\tilde{\mathbf{N}}\right) - s_k\left(\mathbf{H}_{\text{key}}\right)\right| \leq s_1\left(\tilde{\mathbf{N}}\right), \tag{27}$$

Again we consider the leakage as part of the noise, and add the leakage and the measured noise together as $\mathbf{N}_{\text{meas}} = \mathbf{H}_{\text{leak}} + \tilde{\mathbf{N}}$. The ordered singular values for the rank one keyhole matrix, $\mathbf{H}_{\text{key}}$, are

$$\begin{cases} s_k\left(\mathbf{H}_{\text{key}}\right) > 0 & , k = 1 \\ s_k\left(\mathbf{H}_{\text{key}}\right) = 0 & , k > 1 \end{cases}. \tag{28}$$

From (27) and (28) the second largest singular value of the measured keyhole transfer matrix can now be upper bounded as

$$s_2\left(\mathbf{H}_{\text{key}}+\tilde{\mathbf{N}}\right) \leq s_1\left(\tilde{\mathbf{N}}\right). \tag{29}$$

With the variable transformation,

$$\frac{1}{\sqrt{\gamma_{\text{meas}}}}\hat{\mathbf{N}} = \tilde{\mathbf{N}}, \tag{30}$$

where $\hat{\mathbf{N}}$ is normalized as $\left\|\hat{\mathbf{N}}\right\|_{\text{F}}^2 = N_{\text{R}} N_{\text{T}}$ and γ_{meas} is defined in (8), the second largest singular value of the measured keyhole is upper bounded as a function of the measurement SNR and largest singular value of $\hat{\mathbf{N}}$ as

$$s_2\left(\mathbf{H}_{\text{meas}}\right) \leq \frac{s_1\left(\hat{\mathbf{N}}\right)}{\sqrt{\gamma_{\text{meas}}}}, \tag{31}$$

or in terms of eigenvalues

$$\lambda_2\left(\mathbf{W}_{\mathbf{H}_{\text{meas}}}\right) \leq \frac{\lambda_1\left(\mathbf{W}_{\hat{\mathbf{N}}}\right)}{\gamma_{\text{meas}}}, \tag{32}$$

where $\mathbf{W}_{\mathbf{H}_{\text{meas}}}$ is defined in (5) and with

$$s_1\left(\mathbf{H}_{\text{meas}}\right) = \left|\sqrt{\lambda_1\left(\mathbf{W}_{\mathbf{H}_{\text{meas}}}\right)}\right|. \tag{33}$$

This means that *if the second largest singular value of the measured transfer matrix exceeds the threshold (31), we did not measure a keyhole with ideal properties.*

The expectation of the bound is

$$E\left[\lambda_2\left(\mathbf{W}_{\mathbf{H}_{\text{meas}}}\right)\right] \leq \frac{E\left[\lambda_1\left(\mathbf{W}_{\hat{\mathbf{N}}}\right)\right]}{\gamma_{\text{meas}}}, \tag{34}$$

and with the assumption of i.i.d. complex Gaussian entries in $\hat{\mathbf{N}}$, the expectation of the largest singular value of $\hat{\mathbf{N}}$ can be found from the density function of ordered *eigenvalues* [21] of the semi definite Wishart matrix $\mathbf{W}_{\hat{\mathbf{N}}}$,

$$E\left[\lambda_1\left(\mathbf{W}_{\hat{\mathbf{N}}}\right)\right] = \int_0^{\infty} \lambda_1 f_{\Lambda_1}(\lambda_1)\, d\lambda_1. \tag{35}$$

The marginal density function of the largest eigenvalue, $f_{\Lambda_1}(\lambda_1)$, is given in [21].

In Fig. 5 the bound for the mean of the second largest singular value is plotted for different measurement SNRs together with simulated values of the mean of the largest and second largest singular values of an ideal keyhole with measured additive white Gaussian noise, and our measured mean values of the largest and second largest singular values.

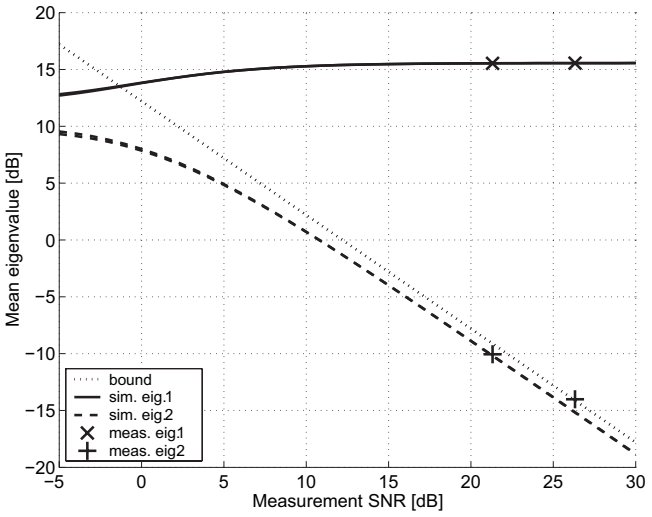

Fig. 5. The mean of the largest and the second largest eigenvalue from simulations together with an upper bound for the second largest eigenvalue, both as a function of the measured SNR. The mean of the eigenvalues from two waveguide measurements with estimated measurement SNRs of $\hat{\gamma}_{meas} \approx$ 21 dB and $\hat{\gamma}_{meas} \approx 26$ dB, are also plotted.

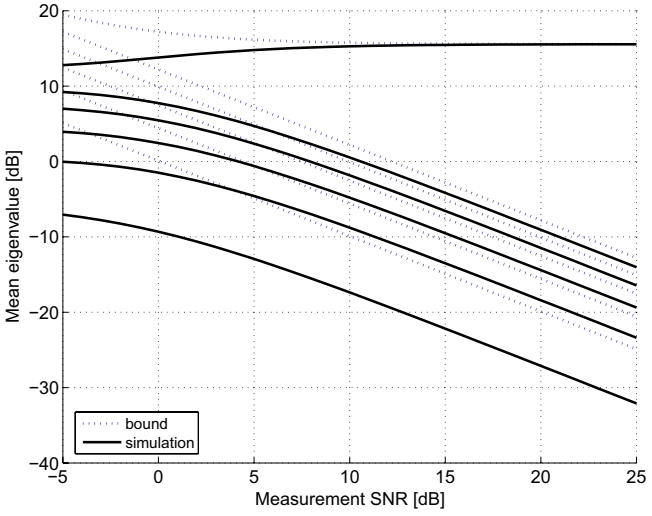

Fig. 6. Simulated mean of the ordered eigenvalues (solid) together with the upper bound (dotted) as functions of measurement SNR, for a 6 x 6 MIMO system.

The singular values, $s_k(\mathbf{H}_{\text{meas}})$, for $k > 2$ could also be bounded by (26). For $k > 1$ there are more than one combination of k and l that fullfills $k+l-1$. It can easily be shown that the tightest one is

$$s_k\left(\mathbf{H}_{\text{key}}+\frac{\hat{\mathbf{N}}}{\sqrt{\gamma_{\text{meas}}}}\right) \leq s_2\left(\mathbf{H}_{\text{key}}\right)+\frac{s_{k-1}\left(\hat{\mathbf{N}}\right)}{\sqrt{\gamma_{\text{meas}}}}. \qquad (36)$$

For a 6×6 MIMO system the eigenvalues and the bounds plotted in Fig. 6. The bound is, however, not very tight for small singular values.

VII. Measurement Results

A. Spatial correlation

As previously discussed, a keyhole channel is defined as a MIMO channels with a low spatial correlation at both the receiver and transmitter side, but still with a low rank (rank one ideally) transfer matrix. In order to demonstrate that a measured channel is a keyhole channel, we first have to separate the capacity reduction (with respect to the i.i.d. case) due to correlation of the antenna signals from the capacity reduction due to the keyhole effect.

Estimates of the full and marginal spatial correlation are presented in this section for the keyhole measurements. The magnitude of the estimated marginal complex spatial correlation (according to (16) and (17)) for neighbouring antenna elements are ~ 0.4 for WG-I, SH and LH at both the transmitter and the receiver side. The correlation does not vary notably with the configuration of the hole, and there is no notable difference between the Kronecker model and the full correlation model.

In (37) and (38) the full correlation matrix for a 2×2 MIMO system (due to space limitations) are estimated according to (15) from the WG-I and LH measurement, respectively.

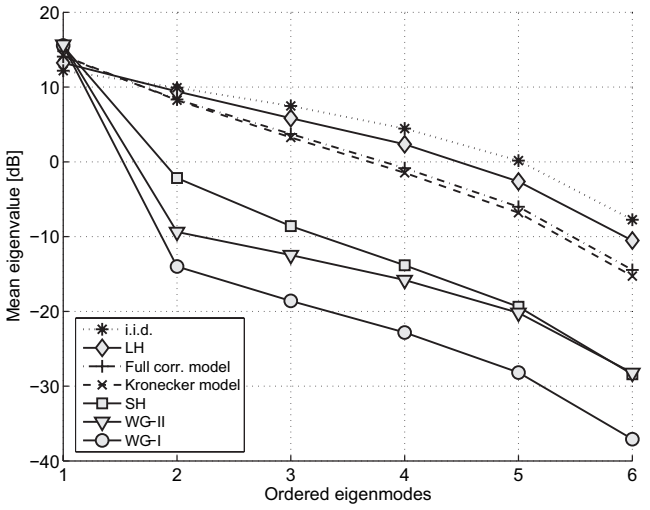

Fig. 7. Mean of the ordered singular values [dB].

B. Eigenvalues

The link gains of the spatial channels in a MIMO system are determined by the eigenvalues of the transfer matrix. In Fig. 7 the mean of the ordered eigenvalues (the diagonal of $\mathbf{\Lambda}$ in $\mathbf{W} = \mathbf{U}\mathbf{\Lambda}\mathbf{U}^{\dagger}$) of a 6×6 MIMO system are presented for different channel setups. The effect of the low rank connection between transmitter and receiver side, realized with a monomode waveguide, is evident. The difference between the means of the largest and second largest eigenvalue is 25 dB and 30 dB for the measured keyholes. As a comparison, the difference between these eigenvalues for the ideal i.i.d. channel is around 2 dB. The difference between the largest and smallest eigenvalues (i.e., the condition number of the matrix $\mathbf{W}$) is almost 50 dB for the WG-I and around 20 dB for the i.i.d. channel. The SH setup also shows a significant difference from the LH and i.i.d. setup. However, the higher-order eigenvalues are still some 10 dB larger for the SH compared to the WG-I. The correlation model (Kronecker) shows the eigenvalue decrease due to receiver and transmitter correlation; LH shows almost the same properties. Except for

$$\hat{\mathbf{R}}_{\text{WG-I}}=\begin{bmatrix} 0.95 & 0.39 & 0.071-j0.39 & 0.024-j0.17 \\ 0.39 & 1.03 & 0.028-j0.18 & 0.076-j0.43 \\ 0.071+j0.39 & 0.028+j0.18 & 0.97 & 0.42+j0.0025 \\ 0.024+j0.17 & 0.076+j0.43 & 0.42-j0.0025 & 1.05 \end{bmatrix} \tag{37}$$

$$\hat{\mathbf{R}}_{\text{LH}}=\begin{bmatrix} 1.04 & -0.0096-j0.059 & -0.30-j0.32 & 0.0091+j0.013 \\ -0.0096+j0.059 & 0.97 & 0.039+j0.029 & -0.29-j0.28 \\ -0.30+j0.32 & 0.039-j0.029 & 1.02 & 0.0082-j0.079 \\ 0.0091-j0.013 & -0.29+j0.28 & 0.0082+j0.079 & 0.97 \end{bmatrix} \tag{38}$$

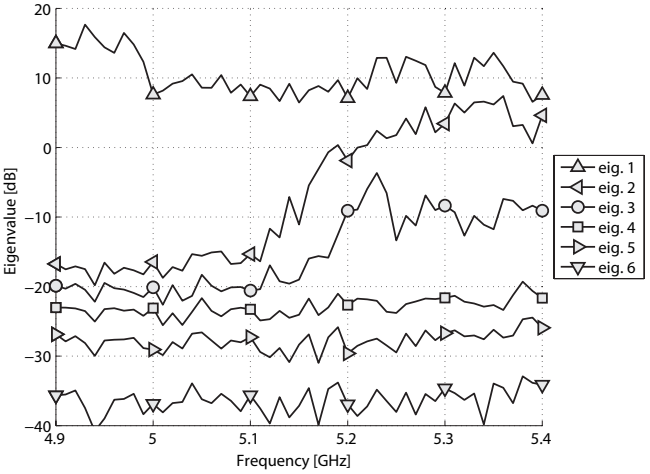

Fig. 8. The 6 eigenmodes plotted over 51 frequency points in the range of $4.9-5.4$ GHz for WG-III.

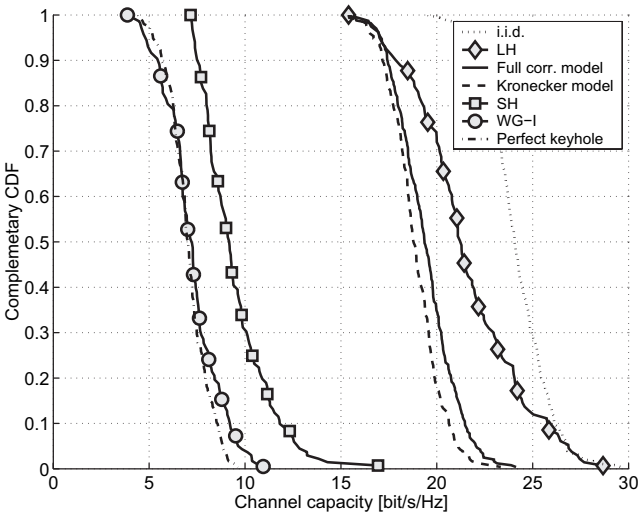

Fig. 9. Channel capacity complementary CDFs for different setups with 6 transmitter and 6 receiver antenna elements.

the largest eigenvalue, the *slope* of the mean eigenvalues for WG follows the i.i.d. curvature, this is due to the fact that the measurement noise is i.i.d.

Fig. 8 shows the distribution of the eigenvalues as a function of the measurement frequency for WG-III. As mentioned in Sec. IV, the attenuation of a propagating mode is small at frequencies above that mode's cut-off frequency; below the cut-off frequency the attenuation is significant and dependent on the length of the wave guide, z, and the frequency distance to the cut-off frequency. This is reflected in the attenuation of the second and third eigenmode in Fig. 8. As the frequency changes, the modes experience a transition from "below cut-off" to "above cutoff". Due to the finite length of our waveguides, the transition is not an abrupt one, but rather extends over a wider frequency range of more than 100 MHz. Note that for our case, the TE20 and the TE01 models have the same cutoff frequency, so that the third eigenmode start to grow at the same frequency as the second eigenmode.

C. Channel capacity

Fig. 9 shows the measured complementary cumulative distribution function (CCDF) of the 6×6 MIMO channel capacities for WG-I, SH and LH configurations at an evaluation SNR of $\gamma_{\text{eval}}=15$ dB. For comparison, the figure also shows the i.i.d. capacity, the full correlation model capacity, the Kronecker model capacity and the capacity for a perfect theoretical keyhole (19). We see that the measured capacity for the WG-I setup is very close to the simulated perfect keyhole. Possible reasons for the differences include (i) noise, (ii) channel variations during the measurements, (iii) residual correlations, (iv) a too small number of channel realizations, and (v) leakage. For the LH scenario, the capacity is close to an i.i.d. channel and the CCDF for its measured capacity is in between the curves for the i.i.d. model and the correlated model. The difference in capacity between the measured WG-I and LH configuration is up to 17 bit/s/Hz. The CCDF for the correlation model shows the decrease in capacity related to the receive and transmit antenna correlation, and shows a capacity that is more than 11 bit/s/Hz higher than the WG-I measurement. With a higher number of channel measurements, the receive and transmit correlation will decrease and therefore the correlation capacity presented serves as a lower limit for the complementary CCDF in the true case.

In Fig. 10 the measured 50% outage capacities versus the number of antenna elements, $N_{\text{R}}=N_{\text{T}}$, are shown for an evaluation SNR of $\gamma_{\text{eval}}=15$ dB. For comparison, the figures also presents the i.i.d. capacity, the correlated capacity and the capacity for a perfect theoretical keyhole. We see that the measured 50% outage capacity for the WG-I setup is very close to the simulated perfect keyhole. With the LH the capacity is close to an i.i.d. channel and its measured capacity is between the curves for the i.i.d. model and the correlated model. With the SH there is some rank reduction, but the length of the hole (2 mm aluminum plate) is too short to attenuate all but one waveguide mode entirely, so that multiple

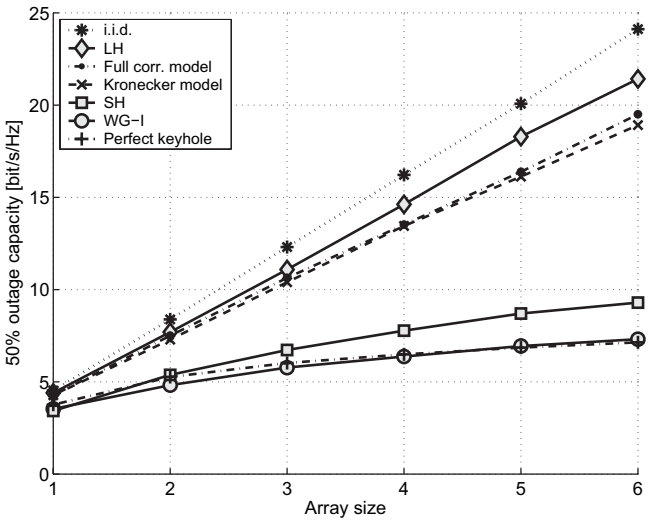

Fig. 10. 50% outage channel capacity vs. the antenna array size, where $N_R = N_T$.

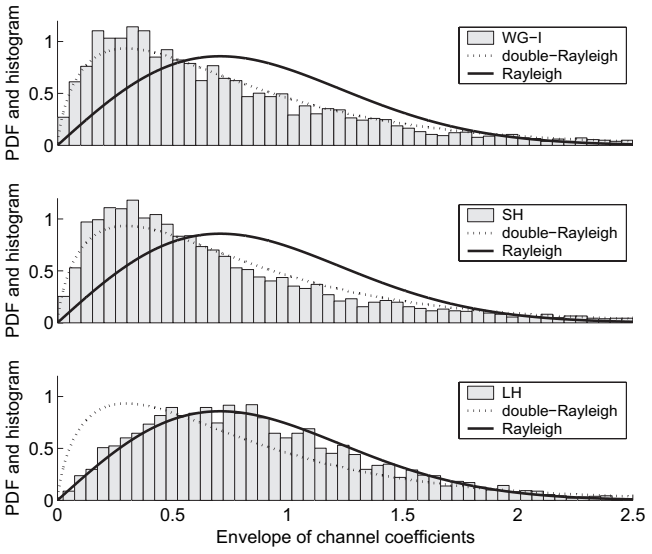

Fig. 11. Envelope distribution for WG-I, SH and LH measurements.

modes can propagate through it. The difference in 50% outage capacity between the measured WG-I and LH configuration is up to 17 bit/s/Hz, for array sizes of 6×6. The correlation model shows the decrease in capacity related to the receive and transmit antenna correlation, and shows a capacity that is more than 11 bit/s/Hz higher than the WG-I measurement. The capacity of the LH increases almost as the capacity for the i.i.d. channel. This shows that the keyhole effect has disappeared entirely when the LH of size 300×300 mm is the (only possible) path between transmitter and receiver.

D. Envelope distribution

Finally, we investigate the statistics of the received amplitudes for the WG-I, SH and LH setups. In Fig. 11 we present histograms of the received amplitudes in the experiment, for the WG-I, SH and the LH cases. As references we also show the PDFs for the amplitude of a complex Gaussian variable (i.e., Rayleigh) and the amplitude of a double complex Gaussian variable (i.e., double-Rayleigh), as given by (20). The received amplitudes with the WG-I correspond well to the double Gaussian distribution, which confirms the predictions of [22], [6], [10]. The received amplitudes for the LH, however, correspond to a Rayleigh distribution since in this case the channel can be described as *one* rich scattering channel.

TABLE I
KOLMOGOROV-SMIRNOV TEST STATISTICS (CUT-OFF AT 0.024)

KS-statistics	Rayleigh	double-Rayleigh
WG-I	0.19	0.021
SH	0.21	0.031
LH	0.022	0.18

In Table I the Kolmogorov-Smirnov (K-S) one-sample test statistics [23] are presented, for the WG-I and the LH setup. At a significance level of 0.01, the K-S test accepts the double-Rayleigh distribution hypothesis. A significance level of 0.01 for the 2520 samples results in a cut-off level at 0.024, i.e. 1 percent of test sets (consisting of 2520 samples) have a D larger than 0.024. For a higher level of significance, (< 0.01) the double-Rayleigh distribution hypothesis will be rejected. A bandwidth of 350 MHz of the measured 500 MHz was used for the test statistics, due to a slight frequency dependence of the antenna gain over a range of 500 MHz. The hypothesis that WG-I follows a double-Rayleigh distribution and that the LH follows a Rayleigh distribution could not be rejected for the given significance level. The hypotheses that SH gives rise to a double-Rayleigh or a Rayleigh distribution are both rejected.

VIII. SUMMARY

In this paper the first conclusive experimental evidence of the keyhole effect in wireless MIMO systems was presented. Using a controlled indoor environment, we found a keyhole with almost ideal properties: the correlations at both the receiver and at the transmitter are low but still the capacity is very low and almost identical to a theoretical perfect keyhole. In our measurements we used two different waveguides, a small hole, and a hole of size 300×300 mm as the only path between two rich scattering environments. For the waveguide cases, we found almost ideal keyhole properties, but for the large hole the capacity is almost as large as for a theoretical Gaussian channel with independent fading between the antenna elements.

We have presented an analysis of the sensitivity of the keyhole measurement with respect to noise and alternative propagation paths, and we presented a bound for the higher eigenmodes as a function of measurement SNR. We found that both the noise and the alternative propagation paths during the channel sounding must be approximately 10 dB weaker than the noise level considered for the capacity computations. Further, multimode propagation as in waveguide channels (e.g., tunnels) are not always (or, more accurately, in most cases are not) keyholes due to multi-mode propagation. From this we can conclude that the keyhole effect due to real-world waveguides like tunnels or corridors will usually be very difficult to measure [24], [25]. This tallies with previous investigations that found that correlation is the main capacity-reducing effect.

ACKNOWLEDGEMENT

Part of this work was financed by an INGVAR grant from the Swedish Foundation for Strategic Research.

REFERENCES

[1] J. H. Winters, "On the capacity of radio communications systems with diversity in Rayleigh fading environments," *IEEE J. Sel. Areas Commun.*, vol. 5, pp. 871-878, June 1987.

[2] G. J. Foschini and M. J. Gans, "On limits of wireless communications in fading environments when using multiple antennas," *Wireless Personal Commun.*, vol. 6, pp. 311-335, 1998.

[3] D. Shiu, G. J. Foschini, M. J. Gans, and J. M. Kahn, "Fading correlation and its effect on the capacity of multi-element antenna systems," *IEEE Trans. Commun.*, vol. 48, pp. 502-513, Mar. 2000.

[4] C. N. Chuah, D. N. C. Tse, J. M. Kahn, and R. A. Valenzuela, "Capacity scaling in MIMO wireless systems under correlated fading," *IEEE Trans. Inf. Theory*, vol. 48, pp. 637-650, Mar. 2002.

[5] A. F. Molisch, M. Steinbauer, M. Toeltsch, E. Bonek, and R. S. Thoma, "Capacity of MIMO systems based on measured wireless channels," *IEEE J. Sel. Areas Commun.*, vol. 20, pp. 561-569, Apr. 2002.

[6] D. Chizhik, G. J. Foschini, and R. A. Valenzuela, "Capacities of multielement transmit and receive antennas: correlations and keyholes," *IEEE Electron. Lett.*, vol. 36, pp. 1099-1100, June 2000.

[7] S. Loyka and A. Kouki, "On MIMO channel capacity, correlations, and keyholes: analysis of degenerate channels," *IEEE Trans. Commun.*, vol. 50, pp. 1886-1888, Dec. 2002.

[8] D. Gesbert, H. Blcskei, D. A. Gore, and A. J. Paulraj, "MIMO wireless channels: capacity and performance prediction," in *Proc. IEEE GLOBECOM 2000*, vol. 2, pp. 1083-1088.

[9] D. Chizhik, G. J. Foschini, M. J. Gans, and R. A. Valenzuela, "Keyholes, correlations, and capacities of multielement transmit and receive antennas," *IEEE Trans. Commun.*, vol. 1, pp. 361-368, Apr. 2002.

[10] D. Gesbert, H. Blcskei, D. A. Gore, and A. J. Paulraj, "Outdoor MIMO wireless channels: models and performance prediction," *IEEE Trans. Commun.*, vol. 50, pp. 1926-1934, Dec. 2002.

[11] D. Chizhik, J. Ling, P. W. Wolniansky, R. A. Valenzuela, N. Costa, and K. Huber, "Multiple-input-multiple-output measurements and modeling in manhattan, *IEEE J. Sel. Areas Commun.*, vol. 21, pp. 321-331, Apr. 2003.

[12] P. Almers, F. Tufvesson, and A. F. Molisch, "Measurement of keyhole effect in a wireless multiple-input multiple-output (MIMO) channel," *IEEE Commun. Lett.*, vol. 7, pp. 373-375, Aug. 2003.

[13] R. R. Mueller, "A random matrix model of communication via antenna arrays," *IEEE Trans. Inf. Theory*, vol. 48, pp. 2495-2506, Sept. 2002.

[14] C. Oestges, B. Clerckx, D. Vanhoenacker-Janvier, and A. Paulraj, "Impact of diagonal correlations on mimo capacity: application to geometrical scattering models, in *Proc. IEEE VTC 2003/Fall*, vol. 1, pp. 394-398.

[15] K. Yu, "Modeling of multiple-input multiple-output radio propagation channels," Licentiate Thesis, July 2002, KTH, Sweden.

[16] S. Loyka and A. Kouki, "New compound upper bound on MIMO channel capacity," *IEEE Commun. Lett.*, vol. 6, pp. 96-98, Mar. 2002.

[17] D. K. Cheng, *Field and Wave Electromagnetics, Second Edition*. Addison.Wesley, 1989.

[18] P. Kyritsi, R. A. Valenzuela, and D. C. Cox, "Channel and capacity estimation errors," *IEEE Commun. Lett.*, vol. 6, pp. 517-519, Dec. 2002.

[19] R. A. Horn and C. R. Johnson, *Topix in Matrix Analysis*. London: Cambridge University Press, 1991.

[20] G. H. Golub and C. F. V. Loan, *Matrix Computations, Second Edition*. London: Johns Hopkins University Press, 1989.

[21] I. E. Telatar, "Capacity of multi-antenna Gaussian channels," *European Trans. Telecommun.*, vol. 10, Nov./Dec. 1999.

[22] V. Erceg, S. J. Fortune, J. Ling, A. J. R. Jr., and R. A. Valenzuela, "Comparisons of a computer-based propagation prediction tool with experimental data collected in urban microcellular environments," *IEEE J. Sel. Areas Commun.*, vol. 15, pp. 677-684, May 1997.

[23] F. J. Massey, The Kolmogorov-Smirnov test for goodness of t," *J. American Statistical Association*, vol. 46, pp. 68-78, Mar. 1951.

[24] S. Loyka, "Multiantenna capacities of waveguide and cavity channels," in *Proc. IEEE CCECE 2003*, vol. 3, pp. 1509-1514.

[25] S. Loyka, "Multiantenna capacities of waveguide and cavity channels, *IEEE Trans. Veh. Technol.*, vol. 54, pp. 863-872, May 2005.

Peter Almers received the M.S. degree in electrical engineering in 1998 from Lund University in Sweden. In 1998, he joined the radio research department at TeliaSonera AB (formerly Telia AB), in Malmö, Sweden, mainly working with WCDMA and 3GPP standardization physical layer issues. Peter is currently working towards the Ph.D. degree at the Department of Electroscience, Lund University. He has participated in the European research initiatives COST273, and is currently involved in the European network of excellence "NEWCOM" and the NORDITE project "WILATI." Peter received an IEEE Best Student Paper Award at PIMRC in 2002.

Fredrik Tufvesson was born in Lund, Sweden in 1970. He received the M.S. degree in Electrical Engineering in 1994, the Licentiate Degree in 1998 and his Ph.D. in 2000, all from Lund University in Sweden. After almost two years at a startup company, Fiberless Society, Fredrik is now associate professor at the department of Electroscience working on channel measurements and modeling for MIMO and UWB systems. His research interests also include channel estimation and synchronization problems for wireless communication, especially for wireless OFDM systems.

Andreas F. Molisch (S'89, M'95, SM'00, F'05) received the Dipl. Ing., Dr. techn., and habilitation degrees from the Technical University Vienna (Austria) in 1990, 1994, and 1999, respectively. From 1991 to 2000, he was with the TU Vienna, becoming an associate professor there in 1999. From 2000-2002, he was with the Wireless Systems Research Department at AT&T (Bell) Laboratories Research in Middletown, NJ. Since then, he has been with Mitsubishi Electric Research Labs, Cambridge, MA. He is also professor and chairholder for radio systems at Lund University, Sweden.

Dr. Molisch has done research in the areas of SAW filters, radiative transfer in atomic vapors, atomic line filters, smart antennas, and wideband systems. His current research interests are MIMO systems, measurement and modeling of mobile radio channels, cooperative communications, and UWB. Dr. Molisch has authored, co-authored or edited four books (among them the recent textbook *Wireless Communications*, Wiley-IEEE Press), eleven book chapters, some 95 journal papers, and numerous conference contributions.

Dr. Molisch is an editor of the *IEEE Transactions on Wireless Communications*, co-editor of a recent special issue on MIMO and smart antennas in the *Journal of Wireless Communications and Mobile Computing*, and co-editor of a recent special issue on UWB in *IEEE Journal on Selected Areas in Communications*.

He has been member of numerous TPCs, vice chair of the TPC of VTC 2005 spring, and will be general chair of ICUWB 2006. He has participated in the European research initiatives COST 231, COST 259, and COST273, where he was chairman of the MIMO channel working group, and is also chairman of Commission C (signals and systems) of URSI (International Union of Radio Scientists). Dr. Molisch is a Fellow of the IEEE and recipient of several awards.